Environmental Pollution 360 (2024) 124685

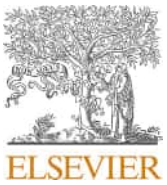

Contents lists available at ScienceDirect

Environmental Pollution

journal homepage: www.elsevier.com/locate/envpol

Binding between Cu^{2+}/Zn^{2+} and aged polyethylene and polyethylene terephthalate microplastics in swine wastewaters: Adsorption behavior, and mechanism insights☆

Mengyu Ma [a], Ruxin Han [a], Ruoqi Han [a], Defu Xu [a], Feihu Li [a,b,*]

[a] Collaborative Innovation Center of Atmospheric Environment and Equipment Technology, Jiangsu Key Laboratory of Atmospheric Environment Monitoring and Pollution Control, School of Environmental Science and Engineering, Nanjing University of Information Science and Technology, 219 Ningliu Road, Nanjing 210044, China

[b] NUIST Reading Academy, Nanjing University of Information Science and Technology, 219 Ningliu Road, Nanjing 210044, China

ARTICLE INFO

Keywords:
Microplastics
Heavy metal
Adsorption behavior
Bridging complexation
Swine wastewaters

ABSTRACT

Microplastics (MPs) have aroused growing environmental concerns due to their biotoxicity and vital roles in accelerating the spread of toxic elements. Illuminating the interactions between MPs and heavy metals (HMs) is crucial for understanding the transport and fate of HM-loaded MPs in specific environmentally relevant scenarios. Herein, the adsorption of copper (Cu^{2+}) and zinc (Zn^{2+}) ions over polyethylene (PE) and polyethylene terephthalate (PET) particulates before and after heat persulfate oxidation (HPO) treatment was comprehensively evaluated in simulated and real swine wastewaters. The effects of intrinsic properties (i.e., degree of weathering, size, type) of MPs and environmental factors (i.e., pH, ionic strength, and co-occurring species) on adsorption were investigated thoroughly. It was observed that HPO treatment expedites the fragmentation of pristine MPs, and renders MPs with a variety of oxygen-rich functional groups, which are likely to act as new active sites for binding both HMs. The adsorption of both HMs is pH- and ionic strength-dependent at a pH of 4–6. Co-occurring species such as humic acid (HA) and tetracycline (TC) appear to enhance the affinity of both aged MPs for Cu^{2+} and Zn^{2+} ions via bridging complexation. However, co-occurring nutrient species (e.g., phosphate and ammonia) demonstrate different impacts on the adsorption, improving uptake of Cu^{2+} by precipitation while lowering affinity for Zn^{2+} owing to the formation of soluble zinc-ammonia complex. Spectroscopic analysis indicates that the dominant adsorption mechanism mainly involves electrostatic interactions and surface complexation. These findings provided fundamental insights into the interactions between aged MPs and HMs in swine wastewaters and might be extended to other nutrient-rich wastewaters.

1. Introduction

Plastic debris wastes, in particular microplastics (MPs, <5 mm in diameter) are omnipresent in both the terrestrial and the aquatic environments (Barnes et al., 2009; Cozar et al., 2014; Tian et al., 2023). A recent projection suggests that approximately 12 billion metric tons of plastic waste will be disposed of or released into the natural environment by 2050 if no interventions are implemented in the current plastic production and waste management policies (Geyer et al., 2017). Such a staggering emission of plastic waste has been posing significant threats and disruptions to the ecosystems and habitats of our planet for decades due to the biotoxicity and the crucial roles of MPs in spreading and enriching toxic substances (e.g., heavy metals (HMs) and organic pollutants), particularly into the food web (Cole et al., 2011; Li et al., 2018a). Specifically, the ability to bind such toxics of MPs endows them with an important vector for transporting these pollutants upward the food chain (Koelmans et al., 2016), leading to health concerns of bioaccumulation and biomagnification, in particular for human beings.

As an important infrastructure to our food chain, livestock farms not only produce meats for human consumption but also raise concerns regarding pollutant exposure, posing significant challenges to global food security. A growing body of evidence indicates that MPs from livestock farms were often consumed as food by livestock (Wang et al., 2020a; Wu et al., 2021; Zhang et al., 2022), rendering livestock meat a

☆ This paper has been recommended for acceptance by Prof. Hefa Cheng.

* Corresponding author.
E-mail address: fhli@nuist.edu.cn (F. Li).

https://doi.org/10.1016/j.envpol.2024.124685
Received 23 May 2024; Received in revised form 3 July 2024; Accepted 5 August 2024
Available online 5 August 2024

critical exposure pathway to microplastics (Kadac-Czapska et al., 2024). This is particularly concerning given that many toxic contaminants, such as antibiotic resistance genes (ARGs), HMs, and organic toxins, accompanied frequently with MPs in livestock farms (Wu et al., 2021; Zhang et al., 2022; Zhu et al., 2019), and that MPs can act as a vector of spreading such pollutants to our food web (Kadac-Czapska et al., 2024; Zhu et al., 2019). Microplastics have been detected in various poultry and livestock meat (Kadac-Czapska et al., 2024; Dong et al., 2023), raising biotoxicity concerns beyond microplastics themselves. Many studies have documented that one critical exposure pathway of HMs to the food web is mediated by microplastics (Kadac-Czapska et al., 2024; Paul et al., 2020; Brennecke et al., 2016).

The binding between MPs and heavy metals under a wide range of environmentally relevant conditions has been extensively explored so far (Brennecke et al., 2016; Bradney et al., 2019; Li et al., 2019; Guan et al., 2020; Liu et al., 2020a; Mao et al., 2020; Binda et al., 2021; Nguyen et al., 2022; Ho et al., 2023; Khan et al., 2024). Apart from many environmental factors (e.g., pH, natural organic matter (NOM), and salinity), the inherent properties of MPs, such as small size, hydrophobicity, high surface area, and abundant surface functional groups, are believed to facilitate the adsorption of heavy metals on MPs (Brennecke et al., 2016; Bradney et al., 2019; Nguyen et al., 2022). Natural and anthropogenic weathering or degradation can greatly alter the surface properties of MPs, thereby affecting their affinity toward HMs (Li et al., 2019; Guan et al., 2020; Liu et al., 2020a; Mao et al., 2020; Binda et al., 2021; Tong et al., 2023). For instance, it was found that the adsorption potential of MPs for cadmium ions (Cd^{2+}) was significantly improved after being biodegraded in a traditional wastewater treatment process (Li et al., 2019). Besides, biofilms formed on MPs can promote their uptake of heavy meals due to the much greater abundance of functional groups (e.g., carboxyl, amino, and phenyl-OH) within the biofilms, which often show higher affinity for heavy metals (Guan et al., 2020; Wu et al., 2022). It was also reported that the adsorption capacities of four aged MPs for copper (Cu^{2+}) and Cd^{2+} ions from seawater were remarkedly enhanced after being weathered by Ultraviolet (UV) irradiation for 3 months (Gao et al., 2021). However, most of the above studies focused on marine environments or sewage treatment scenarios (Li et al., 2022). Few works involved in the interaction between aged MPs and HMs in environmentally relevant scenarios, e.g., swine wastewater (SW), which contains a wide variety of contaminants including ARGs, HMs, tetracycline (TC), dissolved organic matters (DOMs), ammonia, and phosphate (Zhu et al., 2019; Ma et al., 2022). Swine effluents are rich in nutrients and thus often applied as a crucial secondary source for phosphorus recovery through struvite crystallization (Liu et al., 2011; Bah et al., 2023). However, the interactions between aged MPs and HMs in the complex swine wastewater remain poorly understood, which is of significance to elucidate the transport and fate of the HM-MP complexes in the effluents, particularly during the struvite recovery from swine wastewater (Huang et al., 2021).

This study (published as a preprint in Ma and Li, 2023) aims to gain insights into the specific interactions between aged MPs and HM ions, with emphasis on the impacts of the intrinsic properties of MPs and the co-occurring species on the adsorption of HM ions over MPs in swine wastewater. We chose two common microplastics based on abundance and ubiquity in livestock farms (Wu et al., 2021), polyethylene (PE) and polyethylene terephthalate (PET), as model adsorbents to study their adsorption of two typical HMs (also based on abundance), viz. Cu^{2+} and Zn^{2+} in both simulated and real swine wastewaters. To investigate the effects of anthropogenic weathering or aging time on the adsorption of HMs, microplastics with different sizes (1 mm and 50 μm) were aged for 5 and 20 days by the heat persulfate oxidation method before adsorption. The adsorption kinetics and isotherms of heavy metal ions over both pristine and aged microplastics were investigated to illuminate the possible mechanisms controlling the adsorption behavior of both HMs on MPs. The effects of pH, ionic strength, co-occurring tetracycline and humic acid, and ionic competition were also evaluated. This work could provide a fundamental understanding of the roles of aged microplastics in the capture and transport of HMs in nutrient-rich wastewater.

2. Materials and methods

2.1. Chemicals

All chemicals are of analytical grade or higher purity. Potassium persulfate ($K_2S_2O_8$, ≥99.5%), copper chloride dihydrate ($CuCl_2{\cdot}2H_2O$, ≥99.0%), and zinc chloride ($ZnCl_2$, ≥98.0%) were purchased from Sinopharm Chemical Reagent C o., Ltd. (Shanghai, China). Sodium chloride (NaCl, ≥99.5%), humic acid (HA), tetracycline (TC, ≥98.0%), and magnesium ammonium phosphate hexahydrate ($MgNH_4PO_4{\cdot}6H_2O$, ≥98.0%) were obtained from Aladdin Biochemical Technology Co., Ltd. (Shanghai, China). Pristine polyethylene (PE) and polyethylene terephthalate (PET) of *ca.* 1 mm and 50 μm in size were purchased from Wangda Plastic Material Co. (Dongguan, China). All chemicals were used as received, without further purification. Deionized (DI) water was used in the preparation of the solutions. The pH of all solutions was adjusted using sodium hydroxide or hydrochloric acid solutions.

2.2. Weathering of pristine PE and PET microplastics

It has been well documented that the heat persulfate oxidation (HPO) treatment could effectively oxidize microplastics and yield analogical products via similar oxidation pathways as the natural photodegradation, but require less duration (i.e., aging time) than the natural process (Liu et al., 2019). To attain aged microplastics, the HPO method was employed to artificially accelerate the weathering of the original PE and PET. As depicted in Fig. 1a, the pristine PE and PET microplastics were aged in a three-neck flask within a thermostatic water bath at a constant temperature of 70 °C to achieve the optimal oxidation efficiency of $K_2S_2O_8$. An electric stirrer was used to disperse the MP particulates in 100 mM freshly prepared $K_2S_2O_8$ solution (pH 7.0) at a constant speed of 60 RPM, and a Graham condenser was used to prevent the loss of water during the HPO treatment process. The $K_2S_2O_8$ solution was replaced by fresh $K_2S_2O_8$ solution every 12 h due to depletion of the oxidant. The MP samples were separated from the suspension every 2 days and washed 3 times with deionized water before the next cycle of oxidation to avoid the accumulation of K_2SO_4 in the mixture. After being treated consecutively for 5 or 20 days, the aged microplastics (denoted as 'MP-size-weathering time', e.g., PE-50μm-20d) were collected and washed with excessive DI water, followed by freeze-drying and storage in a glass desiccator for further tests.

2.3. Characterization

Fourier transform infrared spectroscopy (FT-IR) was performed by the KBr pellet method using a Nicolet iS5 spectrometer (Thermo Fisher, USA). Before analysis, the MPs especially those of 1 mm in size were frozen in a liquid nitrogen container overnight and then taken out, followed by immediately mixing and grinding with KBr in a clean agate mortar. Scanning electron microscopy (SEM) was performed using a SU1510 microscope (Hitachi, Japan) at an accelerating voltage of 15 kV. The zeta potential of microplastics at different pH was determined using a Zetasizer Nano ZS90 m (Malvern Instruments Ltd., UK). X-ray fluorescence spectroscopy (XRF) data was recorded on a DELTA DC 4000 analyzer (Olympus, USA) by using soil mode. X-ray photoelectron spectroscopy (XPS) analysis was performed on a PHI 5000 spectroscope (Versa Probe, UIVAC-PHI, Japan) using a monochromatized Al Kα X-ray source ($h\nu = 1486.6$ eV). The C 1s region (284.8 eV) was used for calibrating other elements of interest. The three-dimensional (3D) excitation-emission matrix (EEM) fluorescence spectroscopy was conducted on a Cary Eclipse fluorescence spectrophotometer (Agilent Technologies, Inc., USA).

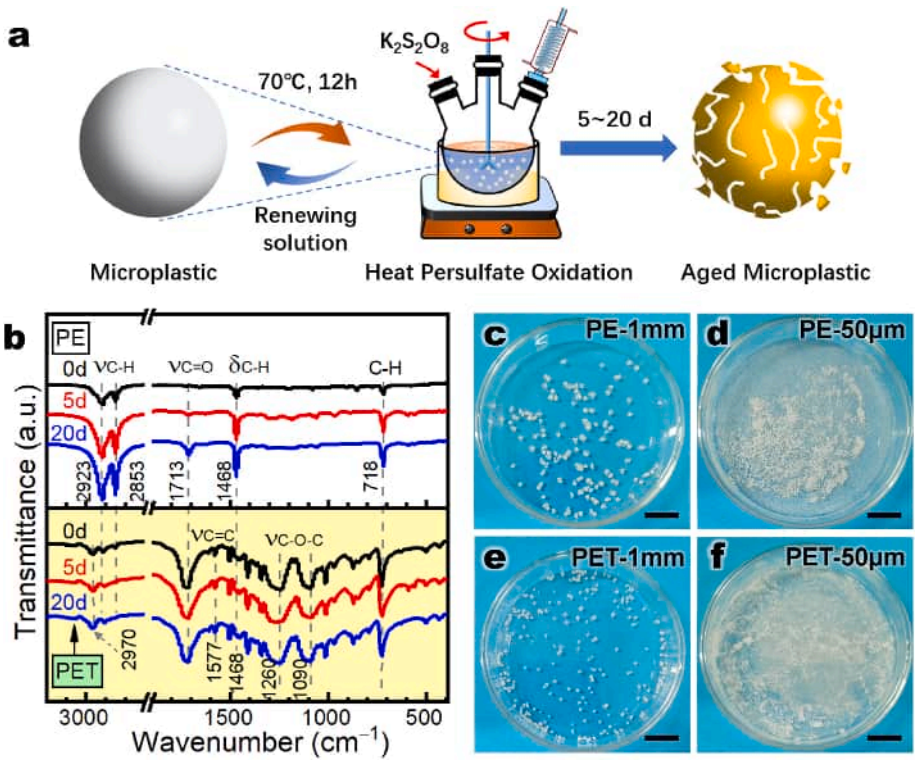

Fig. 1. (**a**) Schematic illustration of the accelerated weathering treatment of pristine PE and PET pellets by heat persulfate oxidation; (**b**) FT-IR spectra of pristine and aged PE and PET as a function of weathering time; (**c**–**f**) Digital images of 20-day-aged PE and PET with different sizes (scale bar = 1 cm).

2.4. Batch adsorption experiments

Adsorption experiments were performed in brown glass vials (20 mL) to avoid the effect of light on the experiments. The stock solutions (100 mg L^{-1}) of Cu^{2+} or Zn^{2+} ions were prepared individually by dissolving the desired amount of copper chloride dihydrate and zinc chloride in deionized water. All adsorption experiments were performed in triplicate at standard atmospheric pressure and a constant room temperature of 20 °C. The effects of microplastic type (i.e., pristine and aged PE and PET), size (1 mm and 50 μm), weathering time (0, 5, and 20 days) on adsorption were performed by adding a desired weight of MPs in 20 mL clean brawn glass bottles containing 10 mL of 5 mg L^{-1} Cu^{2+} or Zn^{2+} at pH 6.0 ± 0.1 with an adsorbent dose of 1 g L^{-1}, followed by capping and mixing on a Labquake tube rotator (Thermo Scientific, USA) at 80 RPM for 48 h. To control a constant pH during adsorption, the mixing was interrupted at 24 and 46 h, respectively, and pH adjustments were immediately performed by dilute hydrochloric acid and sodium hydroxide. Then, the microplastics were recovered by filtering through a 0.22 μm filter, and the supernatant solution was analyzed to determine the Cu^{2+} or Zn^{2+} concentrations on a ZEEnit 700 P flame atomic absorption spectrophotometer (AAS, Analytik Jena GmbH, Germany).

The adsorption capacity of these MPs toward Cu^{2+} or Zn^{2+} ions can be calculated using Eq. (1):

$$q_e = \frac{(C_0 - C_e) \times V}{m} \tag{1}$$

where $\boldsymbol{q}_e$ is the adsorption capacity (mg g^{-1}), m is the mass of the adsorbent (g), $\boldsymbol{C}_0$ is the initial Cu^{2+} or Zn^{2+} concentration (mg L^{-1}), $\boldsymbol{C}_e$ is the heavy metal ion concentration after 48 h of adsorption assuming equilibrium is reached, and $\boldsymbol{V}$ is the total volume of the solution (L).

Likewise, the effects of solution pH (3–6) and ionic strength (0.1 and 1.0 M), co-occurring species including humic acid (HA, 0–100 mg L^{-1}), tetracycline (TC, 0–20 mg L^{-1}), and magnesium ammonium phosphate (MAP, 0–150 mg L^{-1}) on adsorption of Cu^{2+} or Zn^{2+} over two representative MPs (i.e., PE-50μm-20d and PET-50μm-20d) were also investigated in the same manner described above. Additionally, the adsorption kinetic experiments were conducted with the same adsorbent dosage over a contact time ranging from 1.0 to 144 h. The experimental data were fitted with both the pseudo-first and the pseudo-second-order models given in Eqs. (2) and (3):

$$ln(-q_t) = ln\, q_e - k_1 t \tag{2}$$

$$\frac{t}{q_t} = \frac{1}{k_2 q_e^2} + \frac{t}{q_e} \tag{3}$$

where $\boldsymbol{q}_t$ is the adsorption capacity (mg g^{-1}) at contact time $\boldsymbol{t}$ (h), and $\boldsymbol{k}_1$ and $\boldsymbol{k}_2$ are the pseudo-first- and second-order rate constants, respectively. Similarly, the adsorption isotherm tests were carried out over initial Cu^{2+} or Zn^{2+} ion concentrations from 0.1 to 10 mg L^{-1}, at 20, 30, and 40 °C (i.e., 293, 303, and 313 K), respectively. The experimental data were fitted using both the Freundlich and the Langmuir models formulated in Eqs. (4) and (5):

$$q_e = k_F C_e^{1/n} \tag{4}$$

$$q_e = \frac{k_L q_m C_e}{1 + k_L C_e} \tag{5}$$

where $\boldsymbol{k}_F$ (in ($mg^{1-n}\ L^n$) g^{-1}) and $\boldsymbol{n}$ are the Friedrich constants, $\boldsymbol{k}_L$ is the Langmuir adsorption energy constant in L mg^{-1}, and $\boldsymbol{q}_m$ is the theoretical maximum adsorption in mg g^{-1}.

2.5. Mechanism study

To elucidate the mechanism underlying Cu^{2+} or Zn^{2+} ion adsorption over these aged MPs, XRF, FT-IR and XPS analysis of both the 20-day-aged and the Cu^{2+}/Zn^{2+}-loaded MPs were performed in sequence. Besides, as three-dimensional fluorescence excitation-emission matrix (3D-

EEM) spectroscopy is a powerful tool for distinguishing the fluorescence characteristics of organic matter in the aqueous environment, and therefore was used here to evaluate the impact of both HA and TC on the adsorption of Cu^{2+} or Zn^{2+} ions under environmentally relevant conditions. Briefly, the supernatant from adsorption isotherm testing using PE-50μm-20d or PET-50μm-20d as the adsorbent was employed for EEM testing on a Cary Eclipse fluorescence spectrophotometer. The excitation and emission slits were fixed at 10 nm. The excitation wavelength ranges from 200 to 500 nm versus the emission wavelength from 250 to 600 nm. The scanning speed was 1200 nm/min with a wavelength increment of 5 nm. For comparison, the EEM spectrum data of dilute HA and TC solution in the presence or absence of minor Cu^{2+} or Zn^{2+} ions were also collected and analyzed.

3. Results and discussions

3.1. Characterization of pristine and aged MPs

FT-IR analysis is often used to examine the surface functional groups and properties of MPs. Fig. 1b depicts the FT-IR spectra of PE and PET microplastics before and after HPO treatment for different periods. The characteristic FT-IR absorption bands of the pristine PE at 2923, 2853, and 718 cm^{-1} are attributable to the C−H stretching vibration, which was also observed at 2970, 2923, and 718 cm^{-1} for the pristine PET (Reineccius et al., 2023). Besides, the C−H bending vibration of both MPs was detected at 1468 cm^{-1}. Note that the intensity of these absorption bands shows a distinct positive correlation with the weathering time, with the same bands of greater intensity upon weathering for a longer period. This is indicative of fragmentation of the pristine PE by the HPO treatment, which has also been observed earlier (Liu et al., 2019). Interestingly, a new carbonyl absorption peak at 1713 cm^{-1} ($\nu_{C=O}$) occurred on the aged PE with the same trend of the C−H bonds, indicating that the PE microplastics were oxidized and grafted with oxygen-containing functional groups and that the surface oxygen-containing functional groups increased with the weathering time. This observation is consistent with the findings in previous studies (Liu et al., 2019; Gardette et al., 2013). Likewise, the characteristic absorption bands of the pristine PET, e.g., C=C stretching vibration ($\nu_{C=C}$) at 1577 cm^{-1}, and C-O-C stretching vibration (ν_{C-O-C}) at 1260 and 1090 cm^{-1}, exhibited a slight increase in intensity with HPO treatment time, confirming the chemical fragmentation of the pristine PET by HPO treatment (Liu et al., 2019).

Both the original PE and PET microplastics are plain white (Fig. S1), regardless of their particle size. However, the aged MPs, particularly those of 50 μm in size, became slightly pale yellow after a continuous HPO treatment for 20 days (Fig. 1c–f), indicative of changes in the microscopic morphology and structure of these MPs upon HPO treatment. Such structural changes have also been demonstrated by the SEM images shown in Fig. 2. Note that both the pristine PE and PET particulates are nearly spherical with very smooth surfaces (Fig. 2a–d). Upon a consecutive HPO treatment for 5 days, however, both MPs were fragmented into smaller pieces with more irregular surface defects and holes (highlighted by the yellow arrows in Fig. 2b–e). As expected, further increasing the HPO treatment time up to 20 days has resulted in more and finer MP fragments with more abundant surface defects (e.g., cracks, holes, and wrinkles in Fig. 2c–f), which not only verified the above FT-IR results but also greatly increased the specific surface area of these MPs, thereby their affinity for heavy metals (Liu et al., 2020a; Mao et al., 2020; Binda et al., 2021). Based on the SEM observations and the relevant analyses, the morphological evolution (fragmentation process)

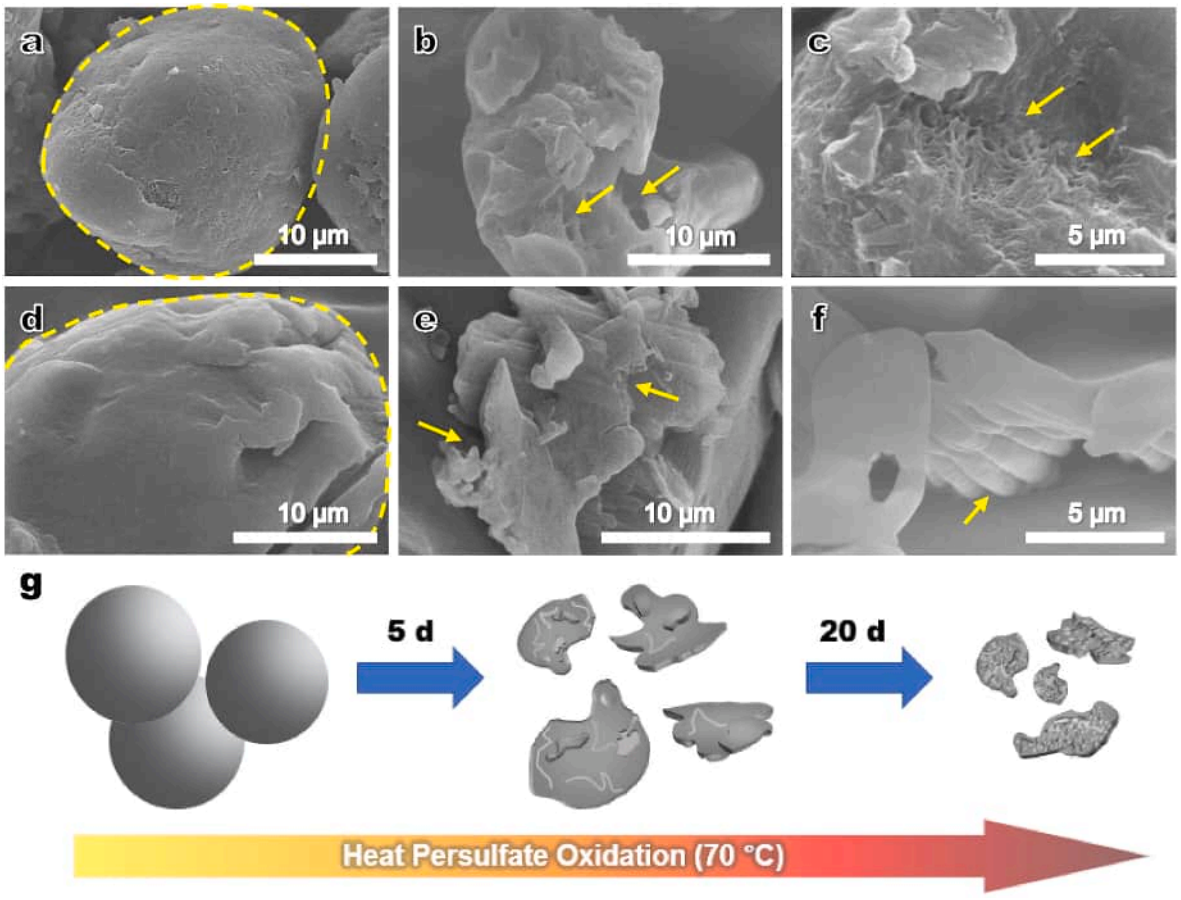

Fig. 2. SEM images of (**a**) pristine PE of 50 μm, (**b**) PE-50μm-5d, (**c**) PE-50μm-20d, (**d**) pristine PET of 50 μm, (**e**) PET-50μm-5d, and (**f**) PET-50μm-20d; (**g**) schematic illustration of the morphological evolution of microplastics during the HPO treatment process.

of microplastics upon HPO treatment is likely to occur in the manner illustrated in Fig. 2g.

The surface charges of MPs play a defining role in their interaction with heavy metals (Mao et al., 2020; Nguyen et al., 2022; Ho et al., 2023). The zeta potential (ζ) of both pristine and aged microplastics were measured in different types of background electrolytes (i.e., NaCl, $CuCl_2$, $ZnCl_2$) and the results are shown in Fig. S2 (Supporting Information). The results showed that the zeta potential of both microplastics decreased with increasing pH, and the pH_{PZC} (point of zero charge) of these microplastics appeared between 3.0 and 4.2, which is consistent with previous report (Zou et al., 2020). Note that weathering by HPO decreased the pH_{PZC} of the two pristine MPs by 0.3–0.8 unit of pH, which is likely due to the introduction of new negatively charged groups to the microplastic surface, i.e., grafting of oxygen-containing groups, thereby shifting the pH_{PZC} of pristine microplastics toward lower pH regions (Zhou et al., 2020). The pH_{PZC} of both the pristine and the aged PET are slightly lower than those of PE (Table S1), indicating that the PET surfaces are more likely to be negatively charged under the same conditions.

3.2. Effects of type, size, and weathering time of MPs on adsorption

To understand the effects of microplastic type, particle size and weathering time on adsorption, the adsorption of Cu^{2+} and Zn^{2+} over two types of MPs, i.e., PE and PET, with particle sizes of 1 mm and 50 μm and weathering time of 5 and 20 days, respectively were investigated comprehensively, and the results are shown in Fig. 3. Obviously, there is little difference in the adsorption capacities of Cu^{2+} and Zn^{2+} of the two MPs of 1 mm under the same conditions regardless of the aging time (the white shading regions in Fig. 3), indicating that the type of MP has little impact on the adsorption affinity in the case of MP of 1 mm in size. With regards to MPs of 50 μm (yellow shading regions), however, both pristine PE and PET demonstrate a slightly higher affinity for Cu^{2+} over Zn^{2+}, with 0.62 mg Cu^{2+} g^{-1} versus 0.57 mg Zn^{2+} g^{-1} for PE, and 0.63 mg Cu^{2+} g^{-1} versus 0.57 mg Zn^{2+} g^{-1} for PET, respectively. Interestingly, as weathering time increased from 5 to 20 days, PE and PET showed different affinities for Zn^{2+} and Cu^{2+}, respectively, with PE adsorbing more Zn^{2+} than Cu^{2+} and PET capturing more Cu^{2+} under the same conditions. This observation is in agreement with a previous report (Wang et al., 2020b) and is likely attributed in part to the much greater abundance of carbonyl groups (−C=O) in aged PET relative to aged PE (Fig. 1b). This functional group tends to form coordination bonds with Cu^{2+} ions preferentially. However, aged PE is rich in polar or charged sites that interact more favorably with Zn^{2+} ions (Wang et al., 2020b). Similarly, it was found that polyamide-6 (PA) and polymethyl methacrylate (PMMA) exhibited higher affinity towards Cu^{2+} than polyvinyl chloride (PVC) and polystyrene (PS) (Yang et al., 2019), whereas PS appeared to enhance the bioavailability of Cu^{2+} and Zn^{2+} in soil systems (Ma et al., 2023).

Moreover, it was noted that MPs of 50 μm demonstrated much greater adsorption capacities for both heavy metals than their counterparts of 1 mm under the same conditions, which is because the smaller the particle size, the larger its specific surface area, and therefore the more active sites for bonding heavy metal ions. This observation is in good agreement with those reported elsewhere (Nguyen et al., 2022; Wu et al., 2022; Ma et al., 2022). In addition, it was well documented that microplastics of smaller size, particularly the nanoplastics can not only enhance the adsorption affinity toward HM species (Alimi et al., 2018),

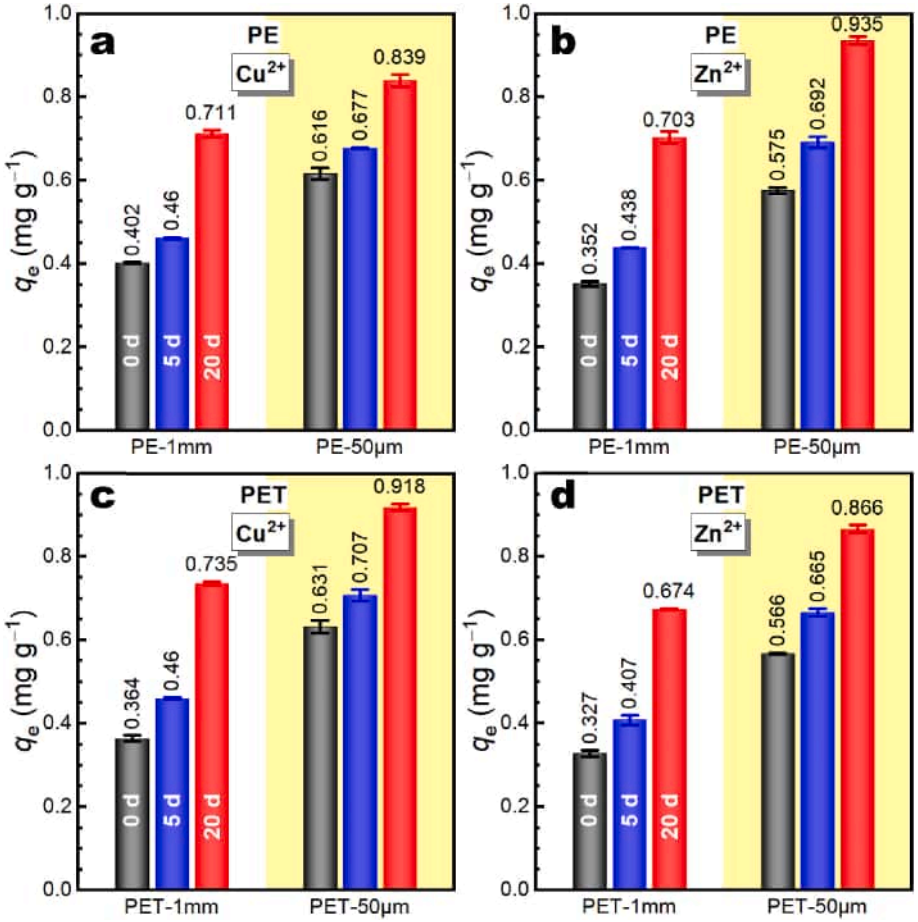

Fig. 3. Effects of microplastic type, size, and weathering time on Cu^{2+} and Zn^{2+} adsorption. (**a**) Cu^{2+} adsorption over PE, (**b**) Zn^{2+} adsorption over PE, (**c**) Cu^{2+} adsorption over PET, and (**d**) Zn^{2+} adsorption over PET.

but also increase the overall kinetics of their reactivity toward aquatic contaminants and thereof the intraparticulate contaminant diffusion (Town et al., 2023). Besides, it was found that prolonging the weathering time can result in greater adsorption capacities of the aged MPs for both heavy metals, in good agreement with earlier reports (Liu et al., 2020a; Al Harraq et al., 2022). This is as expected since extending the weathering time can lead to a higher degree of fragmentation and produce more defect-rich MP fragments with high dispersibility (Al Harraq et al., 2022; Duan et al., 2021), thereby offering more sites (e.g., oxygen-containing functional groups) (Reineccius et al., 2023) for the adsorption of heavy metals. In light of the adsorption capacity, PE-50μm-20d and PET-50μm-20d with the maximum adsorption capacities for both heavy metals, i.e., 0.84 and 0.92 mg Cu^{2+} g^{-1} for PE (Fig. 3a–c) and 0.94 mg g^{-1} and 0.87 mg Zn^{2+} g^{-1} for PET (Fig. 3b–d), were selected for the subsequent batch adsorption experiments.

3.3. Effects of pH and ionic strength

It is well-known that electrostatic interactions play an important role in the adsorption of heavy metal ions on MP adsorbents (Wang et al., 2020b; Wang et al., 2022). Fig. 4 shows the effects of solution pH and ionic strength on the adsorption of Cu^{2+} and Zn^{2+} over the two aged MPs, PE-50μm-20d and PET-50μm-20d. The adsorption of both Cu^{2+} and Zn^{2+} over the two aged MPs showed a gradual increase as the solution pH increased from 3 to 4, followed by a steep increase at pH 4−6. This observation is reasonable and expected since the surfaces of PE and PET are positively charged when the solution pH is less than their pH_{PZC} (Fig. S2), leading to relatively lower adsorption of Cu^{2+} and Zn^{2+} due to the Coulomb repulsion between the adsorbents and the adsorbates. As the pH rises beyond their pH_{PZC} (i.e., pH >4, Table S1), the PE and PET surfaces are negatively charged with increasing pH (Fig. S2), which is more favorable for the adsorption of positively charged heavy metal ions via the Coulomb attraction. This also explains the rapid increase in adsorption capacity at pH 4−6. Similar trends have also been observed for the adsorption of metal ions on other MPs (Nguyen et al., 2022; Wang et al., 2019) as well as nanomaterials (Zhao et al., 2011).

Ionic strength (***I***) dependence of adsorption has been widely used, in conjunction with the pH effect, to indirectly deduce the underlying adsorption mechanisms between the adsorbents and the adsorbates (Goldberg, 2014). Strong inner-sphere surface complexes were believed to form for ions with little ionic strength dependence; weak outer-sphere surface complexes were deemed to form for ions showing marked ionic strength dependence. Note that the adsorption of Cu^{2+} on both MP adsorbents demonstrated little ionic strength dependence over the pH ranging from 3 to 4 (Fig. 4a–c), indicating the probable formation of inner-sphere surface complexes between Cu^{2+} and the surface carboxyl groups of both aged MPs. As pH rises beyond 4, the Cu^{2+} adsorption on both aged MPs was dependent on the ionic strength, with relatively lower adsorption capacities at higher ionic strength (1.0 M NaCl) due to the remarked competition from sodium ions (Na^{+}) in solution. This phenomenon is indicative of the formation of weak outer-sphere surface complexes of Cu^{2+} on both aged MPs surfaces over the pH range of 4–6. In other words, the Coulomb attraction is the dominant mechanism responsible for Cu^{2+} uptake over pH 4−6. These results of ionic dependence are in good agreement with previous studies (Fu et al., 2021; Wang et al., 2021a; Lu et al., 2022).

Likewise, the competition from Na^{+} ions in a solution of higher ionic strength with Zn^{2+} for adsorption is remarkable, leading to a great

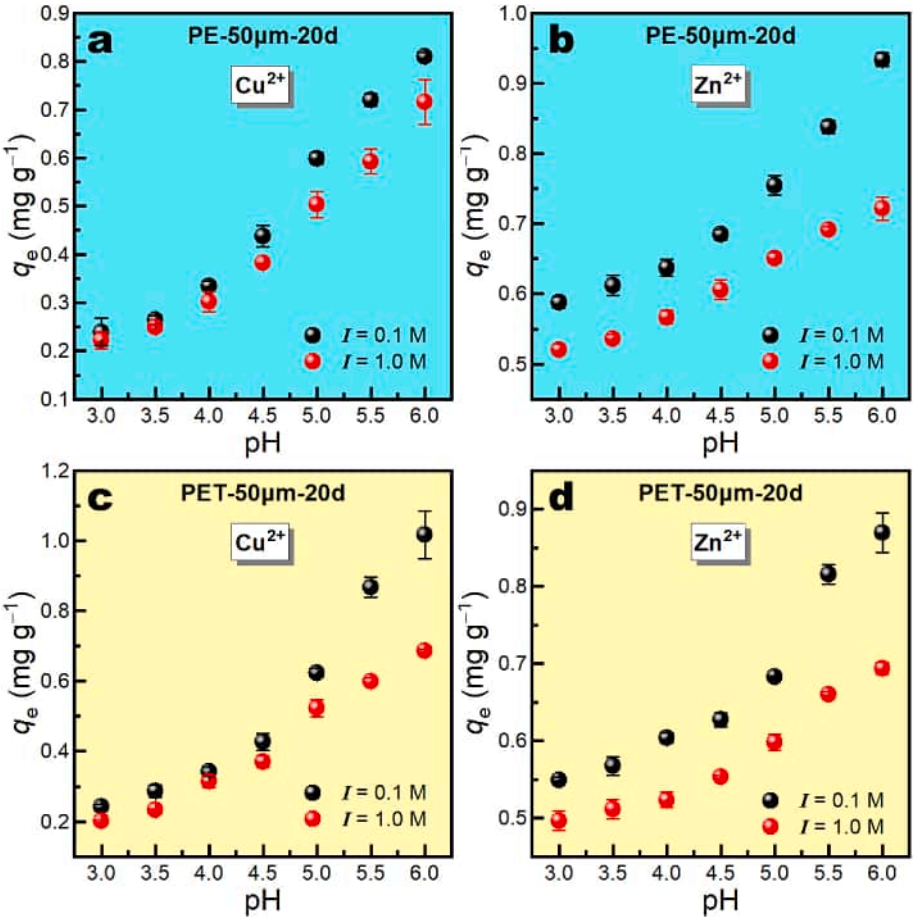

Fig. 4. Effects of pH and ionic strength (***I***) on Cu^{2+} and Zn^{2+} adsorption over the two aged MPs. (**a**) Cu^{2+} adsorption over PE-50μm-20d, (**b**) Zn^{2+} adsorption over PE-50μm-20d, (**c**) Cu^{2+} adsorption over PET-50μm-20d, and (**d**) Zn^{2+} adsorption over PET-50μm-20d.

recession in the adsorption capacity of Zn^{2+}. For example, the adsorption of Zn^{2+} on PE decreased from 0.93 mg g^{-1} with $I = 0.1$ M NaCl to 0.72 mg g^{-1} with $I = 1.0$ M and from 0.87 mg g^{-1} to 0.69 mg g^{-1} on PET at pH 6. Such a distinct ionic strength dependence of Zn^{2+} adsorption on both aged MPs over the pH range of 3–6 suggests the formation of weak out-sphere surface complexes of Zn^{2+} on both aged MPs surfaces. Furthermore, according to the DLVO theory, increasing the ionic strength of the solution could compress the bilayer over the adsorbent surface and thereby decrease the corresponding electrostatic repulsion, leading to increased aggregation of microplastics and a decrease in accessible adsorption sites, which further reduces the adsorption somewhat (Alimi et al., 2018; Li et al., 2018b).

3.4. Effects of co-occurring species

Recall that swine effluents are complex and rich in DOMs, antibiotics, and nutrient components (e.g., ammonia, and phosphate). Therefore, the following section focuses on evaluating the impacts of these co-occurring species on the adsorption of both Cu^{2+} and Zn^{2+} over the two aged MPs by employing HA as model DOM, TC as model antibiotic, and magnesium ammonia phosphate (MAP) ions as model nutrient components. Considering that leaching of DOMs from MPs often requires strong weathering conditions such as a long-term exposure to sunlight or UV irradiations (Barhoumi et al., 2023; Lee et al., 2021), it is believed that the amount of MP-derived DOM is negligible during the adsorption process at 20 °C.

3.4.1. Effect of HA

DOMs are widespread in livestock effluents and inevitably interact with MPs, which is believed to influence the adsorption of heavy metals (Zou et al., 2020) and other co-occurring contaminants (Abdurahman et al., 2020). HA has been reported to account for 50–75% of DOM in the natural environment (Shabbir et al., 2022) and therefore was chosen as model DOM to explore its impact on the adsorption of heavy metals over the two aged MPs (Figs. S3a and b). As HA contents increased from 0 to 100 mg L^{-1}, the adsorption of both heavy metals on the two aged MPs increased obviously. For instance, the adsorption of Cu^{2+} on PE-50μm-20d was improved by 112.5%, from 0.8 to 1.7 mg g^{-1}, in the presence of 100 mg L^{-1} of HA as compared to that without HA (Fig. S3a). Similar enhancements in the adsorption potential of heavy metals were also observed for Pb^{2+} adsorption on polystyrene (PS) in either a simulated effluent (Lu et al., 2022) or in a real sewage scenario (Li et al., 2019).

The facilitation of heavy metals adsorption over MPs by HA is believed to be attributed to the bridging attraction of HA in the adsorption process (Nguyen et al., 2022; Li et al., 2018b). It was shown that heavy metal ions are apt to combine with the carboxyl and hydroxyl groups of HA molecules through surface complexation, ion exchange, and electrostatic interactions to form stable HM-HA complexes (Yang et al., 2015), which then are likely to bond with MPs through intermolecular bridging attraction, thereby boosting to adsorption of heavy metals onto MPs.

3.4.2. Effect of TC

TC is a common veterinary antibiotic that is widely used on livestock farms. It is well-defined that the interactions between TC and MPs can significantly alter the surface of MPs, which in turn changes the bioavailability, bioaccumulation, and fate of TC in aquatic environments (Wang et al., 2021a; Torres et al., 2021). The effect of co-occurring tetracycline (TC) on the adsorption of heavy metals over the two aged MPs (PE-50μm-20d, and PET-50μm-20d) was investigated and the results are given in Figs. S3c and d. Note that the adsorption of Zn^{2+} on both MPs did not increase so much as the TC concentration increased from 0 to 20 mg L^{-1} (Fig. S3d), while the adsorption of Cu^{2+} on aged PET increased profoundly with increasing TC (yellow shaded region in Fig. S3c), with a 2.3-fold increase in the adsorption capacity of Cu^{2+} in the presence of 20 mg L^{-1} TC relative to that without TC. This observation indicates that a high concentration of TC significantly promotes Cu^{2+} adsorption over aged PET, which is likely due to the strong complexation reaction between Cu^{2+} and TC (Wang et al., 2021b) and the bridging ability of TC to bind up the resulting Cu-TC complexes with the aged PET (Zhang et al., 2015). Similar observations have also been reported elsewhere (Tong et al., 2023; Yu et al., 2020). It was also found that the presence of TC remarkedly improved the adsorption of Cu^{2+} on MPs while demonstrating almost no effect on the adsorption of Zn^{2+} on the same MPs due to the weak complexation between Zn^{2+} and TC (Lin et al., 2021). The weak complexation affinity of Zn^{2+} with TC leads to a relatively small bridging enhancement and thus little increase in the adsorption of Zn^{2+} over the two aged MPs in the presence of TC.

3.4.3. Effect of MAP ions

Likewise, the effect of co-occurring MAP ions (i.e., Mg^{2+}, NH_4^+, and PO_4^{3-}) on the adsorption of both heavy metals over the two aged MPs was studied in simulated effluents (Figs. S3e and f). Interestingly, MAP ions showed opposite effects on the adsorption of Cu^{2+} and Zn^{2+} on the two aged MPs, with the adsorption of Cu^{2+} increasing with MAP concentration and Zn^{2+} adsorption on the two aged MPs decreasing with MAP concentration. For example, the adsorption of Cu^{2+} on aged PET was improved by 200%, from 0.90 to 2.73 mg g^{-1}, in the presence of 10 mg L^{-1} MAP compared to that in the absence of MAP ions (yellow shaded region in Fig. S3e). This is likely to be attributed to the reaction between Cu^{2+} and PO_4^{3-} to form sparingly-soluble copper phosphate ($Cu_2(PO_4)_3$) precipitates, resulting in a significant reduction in the content of dissolved Cu^{2+} in solution. Similar observations have also been reported previously (Huang et al., 2020). However, in the case of Zn^{2+}, even zinc phosphate is also sparingly soluble in water, but the presence of NH_4^+ ions in the simulated solution is likely to boost the dissolution of such compound because of the formation of more soluble zinc ammine complexes (Frazier et al., 1975). Moreover, it is believed that the presence of Mg^{2+} appears to induce the agglomeration of both aged MPs via the cationic bridging (Upadhyay et al., 2022; Liu et al., 2020b), which certainly reduces the abundance of active sites and consequently their adsorption capacity for Zn^{2+}.

3.5. Adsorption kinetics

To understand the adsorption behavior and the competition between the two heavy metals, adsorption kinetics were studied in both the unary and the binary adsorptive systems at an initial pH of 6 using both the pristine and the aged MPs as adsorbents. Intuitively, regardless of the type of adsorbent and adsorbate as well as the unary or binary adsorbate system, all adsorption kinetic data demonstrated a clear logarithmic relationship with the contact time (Fig. 5 and Fig. S4). Specifically, the adsorption of Cu^{2+} or Zn^{2+} ions on both the pristine and the aged MPs was highly rapid in the initial stage (within 0–25 min), followed by a slow adsorption stage (25−50 min) until an adsorption equilibrium was reached (>50 min). For example, after 25 min of adsorption, the adsorption capacity of Cu^{2+} on PET-50μm-20d attained up to 0.79 mg g^{-1}, accounting for 86% of the capacity (i.e., 0.92 mg g^{-1}) after adsorption for 2.5 h when an adsorption equilibrium was assumed to be reached. Concerning other adsorption processes, it was found that all the adsorption capacities of the initial stages have attained over 85% of the corresponding equilibrium capacity, indicating that the adsorption rates of Cu^{2+} and Zn^{2+} on these MPs were quite fast and that most of the adsorption was essentially accomplished in the initial rapid adsorption stage. Similar biphasic adsorption behavior was also observed in the case of Cu^{2+} captured by UV-aged PS particles (Chen et al., 2022), and the initial rapid adsorption is believed to be ascribed to chemical reaction and film diffusion processes (Yan et al., 2023). Moreover, the high difference in concentration of Cu^{2+} or Zn^{2+} ions between the bulk solution and the adsorbent surface appears to boost a large mass transfer

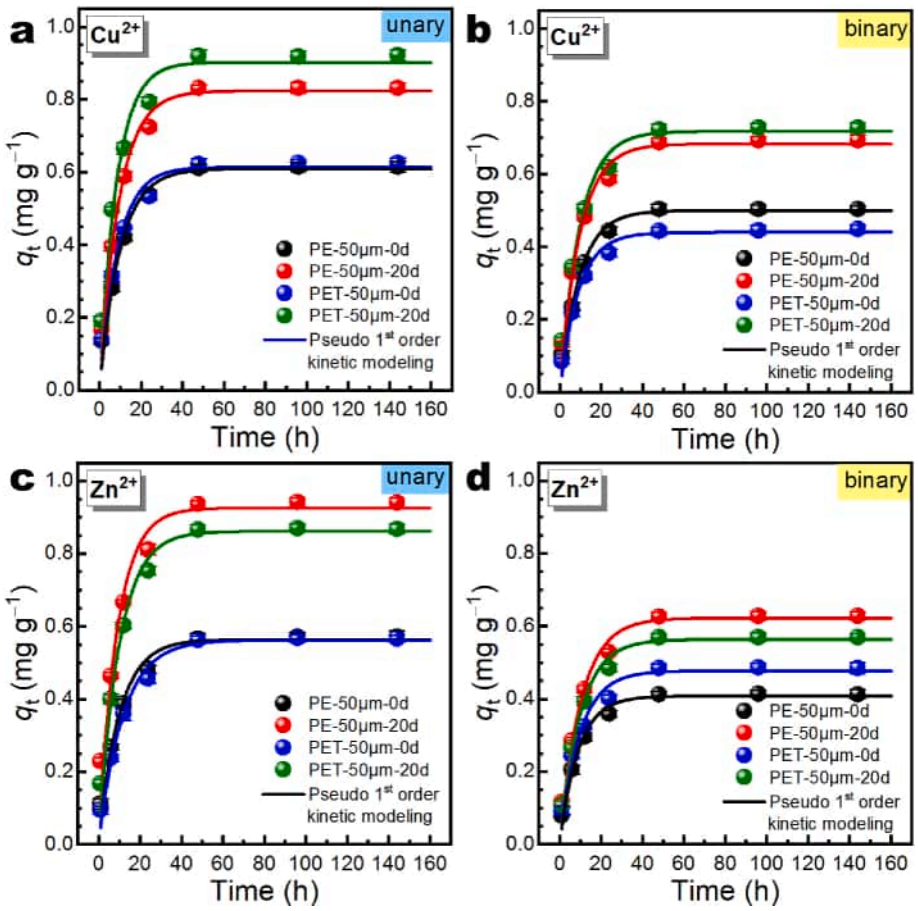

Fig. 5. Adsorption kinetics of Cu^{2+}/Zn^{2+} over both the pristine and the aged MPs in unary/binary adsorptive systems with Pseudo-1st-order kinetic modeling. (**a**) Cu^{2+} onto MPs in unary systems, (**b**) Cu^{2+} onto MPs in binary systems, (**c**) Zn^{2+} onto MPs in unary systems, and (**d**) Zn^{2+} onto MPs in binary systems (adsorbent dosage = 1 g L^{-1}, pH = 6, T = 20 °C; in unary adsorptive systems, initial Cu^{2+} or Zn^{2+} ($C_{0\text{-}Cu}$/$C_{0\text{-}Zn}$) = 5 mg L^{-1}; in binary adsorptive systems, $C_{0\text{-}Cu}$ = $C_{0\text{-}Zn}$ = 5 mg L^{-1}).

during the initial stage of adsorption, resulting in an initial rapid adsorption (Chen et al., 2021).

Interestingly, it is evident by comparing the adsorption in both the unitary and the binary adsorptive systems that there was a strong competition between Cu^{2+} and Zn^{2+} for binding sites (Fig. 5 and Fig. S4), irrespective of the type of adsorbents and their degree of weathering. This phenomenon is indicative of the adsorption of both heavy metals over these MPs was governed by the same mechanism. To identify the adsorption behaviors of both HM ions over these MP adsorbents in real swine wastewater systems, adsorption kinetic experiments were also conducted in real swine wastewater of highly complex compositions (Table S2). It was found that the adsorption kinetic trends of both ions were essentially unaffected by the actual swine wastewater, except that the corresponding adsorption capacities were reduced to varying degrees (Fig. S5), possibly due to the competition from the co-occurring calcium (Ca^{2+}) and magnesium (Mg^{2+}) ions. In addition, the preference of both aged MPs toward different heavy metals, i.e., aged PE prefers to adsorb Zn^{2+} ions while aged PET prefers Cu^{2+} ions, was also observed in both unitary and binary adsorptive systems (Fig. 5, Figs. S4 and S5), which is good agreement with the above results shown in Fig. 3.

Fitting of the kinetic data using both the pseudo-first-order (Eq. (2)) and the pseudo-second-order (Eq. (3)) models suggested that the best-fit kinetic parameters (Tables S3 and S5), particularly all the correlation coefficients (R^2) are >0.95, implying that both kinetic models are capable of well describing the adsorption behavior of both heavy metals on these MPs (Fig. 5, Figs. S4 and S5). Further comparisons revealed that R^2 values obtained from the pseudo-second-order model were a bit greater than those from the pseudo-first-order model for both heavy metals (Tables S3 and S4), indicating that the former is more suitable for describing all these adsorption kinetic data and that the adsorption of Cu^{2+} and Zn^{2+} over these MPs was governed by a chemisorption process (Yan et al., 2023).

3.6. Adsorption isotherms

To evaluate the effect of temperature on Cu^{2+} and Zn^{2+} adsorption and estimate the theoretical maximum adsorption capacity (q_m) of these MPs, both the Freundlich (Eq. (4)) and the Langmuir (Eq. (5)) models are applied to the equilibrium adsorption data in both the unary and the binary adsorptive systems (Figs. S6 and S7). The best-fit isotherm parameters for both models are tabulated in Tables S5 and S6. Note that the best-fit R^2 values calculated from both the Langmuir model (0.994−0.999) and the Freundlich model (0.981−0.997) are relatively close to 1, indicating that both models can accurately describe the adsorption process at different temperatures (i.e., 293, 303, and 313 K). However, R^2 values obtained from the Langmuir model were slightly greater than those from the Freundlich model for both the unary and the binary adsorptive systems, suggesting that the former model is better in defining these adsorption isotherm data and that both heavy metal ions were likely to occur in a monolayer manner based on the basic assumption of the Langmuir model (Sparks et al., 2023).

Additionally, the parameter n calculated from the Freundlich model is often used as an indicator of the easiness or likeliness of a specific adsorption process, with n >1 indicative of a favorable adsorption

process (Shen et al., 2021). Note that all the ***n*** values are above 1, suggesting that the adsorption of Cu^{2+} and Zn^{2+} ions over both aged MPs are favorable and easy to proceed under the given conditions, in good agreement with previous reports (Nguyen et al., 2022; Wang et al., 2020b; Chen et al., 2022; Qiao et al., 2019). Moreover, the adsorption of both metal ions over these aged MPs was affected by temperature, with a higher adsorption capacity under high-temperature conditions (Tables S5 and S6). Generally, the greater adsorption capacity at higher temperatures implies that adsorption is an endothermic process, otherwise, the adsorption is exothermic. The isotherm data at different temperatures suggest that the adsorption of both heavy metal ions on the two aged MPs was endothermic, in good agreement with the results of previous studies (Binda et al., 2021; Nguyen et al., 2022; Wang et al., 2020b; Wang et al., 2022). Consistent with the adsorption kinetic results, the adsorption of either Cu^{2+} or Zn^{2+} in the binary adsorptive systems was lower than that in the unary adsorptive systems under the same conditions (Figs. S6 and S7), indicating that competition between Cu^{2+} and Zn^{2+} ions occurred during the adsorption process, particularly in the binary adsorptive systems.

3.7. Adsorption mechanisms

To elucidate the mechanism responsible for Cu^{2+} and Zn^{2+} adsorption over both aged MPs, spectroscopic analysis was conducted on both MP samples (i.e., PE-50μm-20d and PET-50μm-20d) before and after adsorption (Fig. 6 and Figs. S8−10). Each heavy metal ion was successfully captured by both aged MPs after 48-h of contact at pH 6, as indicated by the appearance of $K_{\alpha1}$-and $K_{\alpha2}$-shell emission lines of either Cu^{2+} or Zn^{2+} after adsorption (Fig. 6a; Fig. S8a). Besides, the intensity of absorption peaks at 1713 cm^{-1} of both aged MPs and 3430 cm^{-1} (attributable to the stretch vibration of surface hydroxyls) of the aged PET has changed apparently upon adsorption of either Cu^{2+} or Zn^{2+} ions (Fig. 6b; Fig. S8b), implying both the carboxyl and the surface hydroxyl groups are involved in the adsorption of both heavy metals, in good agreement with previous reports (Wang et al., 2020b; Yang et al., 2019). Such MPs-HMs interactions are most likely to be physical due to the absence of new peaks and no shifts in the above peaks (Wang et al., 2022; Zhao et al., 2021), which is also consistent with the above speculation about the dominant adsorption mechanism based on the results of ionic strength dependence (Fig. 4). XPS analysis of Cu- and Zn-loaded MPs indicated that both Cu^{2+} and Zn^{2+} ions were bound over the surface of both MPs without chemical valence changes, as evidenced by the

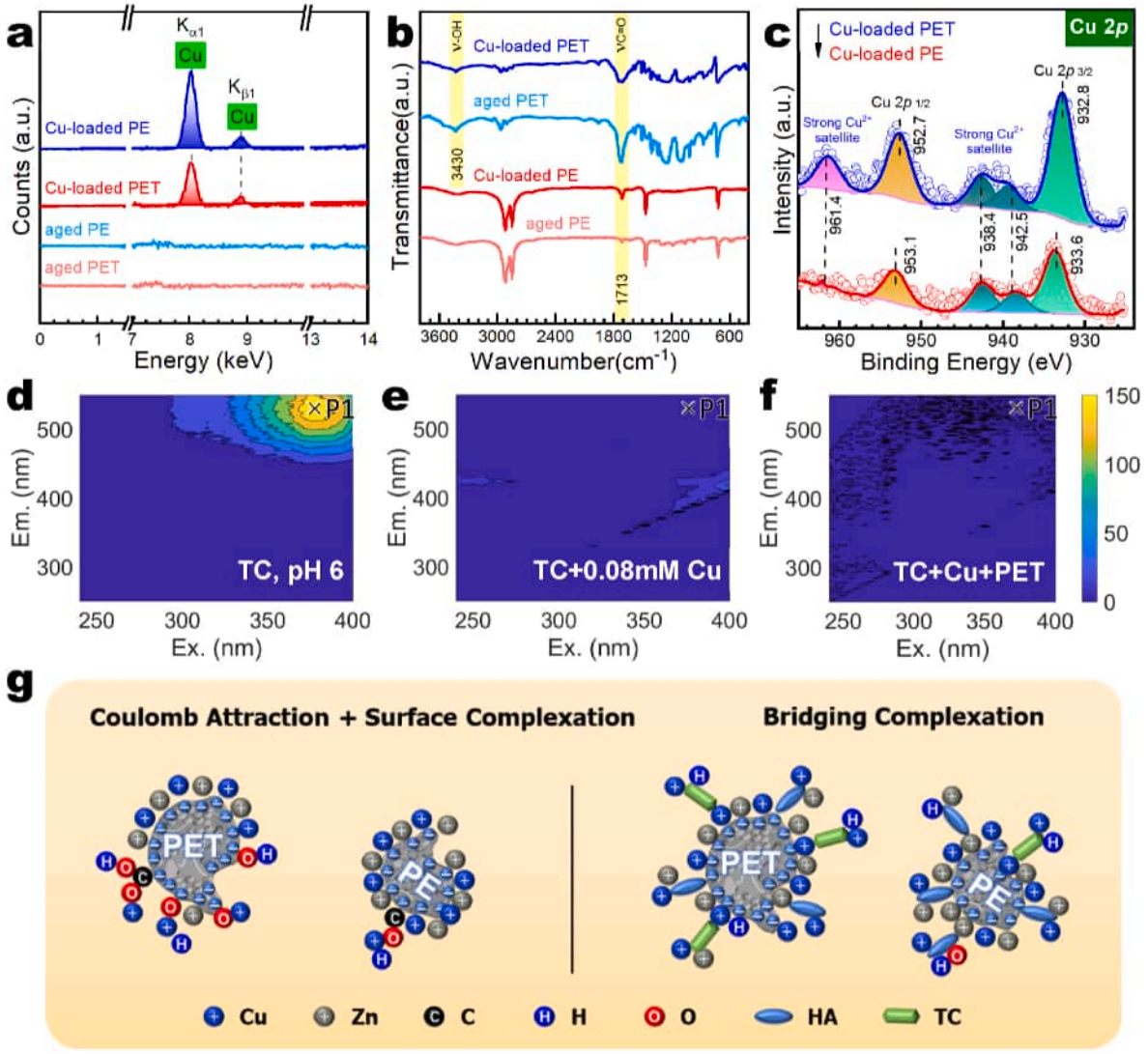

Fig. 6. (**a**) XRF and (**b**) FT-IR spectra of 20-day-aged MPs (i.e., PE-50μm-20d and PET-50μm-20d) before and after adsorption of Cu^{2+} at pH 6; (**c**) Cu 2p XPS region of Cu-loaded aged PE and PET; 3D-EEM spectra of (**d**) TC at pH 6, (**e**) TC + 0.08 mM Cu^{2+}, and (**f**) TC + 0.08 mM Cu^{2+} + 0.1 g L^{-1} PET; (**g**) the proposed adsorption mechanisms in the absence (left) or presence of HA and TC (right).

characteristic XPS peaks in the Cu 2p (Fig. 6c) and Zn 2p regions (Fig. S8c). The O1s regions can be deconvoluted into O-M-O (~530.5 eV, M = Cu or Zn), (C=O)-O-M (~532 eV), and (C=O)-O-M-OH (~533 eV), respectively (Fig. S8d–e), corresponding to the coordination modes of chelating, monodentate, and pseudo-bridging bidentate as indicated elsewhere (Pérez et al., 2022). This is in good agreement with the above FT-IR spectra (Fig. 6b; Fig. S8b), demonstrating both surface hydroxyl and carbonyl groups were involved in the binding of Cu^{2+} and Zn^{2+} over the aged PE and PET.

The 3D-EEM fluorescence spectra of TC and HA were studied respectively in the presence of HMs, and/or MPs to explore the impacts of both co-occurring species on adsorption (Fig. 6d–f, S9, S10). The peak at Ex/Em = 375/526 nm (P1, Fig. 6d–f, S9) is the characteristic fluorescence spectrum of TC (Meng et al., 2020), whereas the peaks at Ex/Em = 260/464 nm (P1, Fig. S10), 295/532 nm (P2), and 235/450 nm (P3) are attributed to the humic-like compounds in HA (Tang et al., 2019; Ateia et al., 2017). Note that the fluorescence intensity of TC or HA decreased obviously in the presence of individual HM or MP species (Fig. 6f; Figs. S9 and S10), indicative of fluorescence quenching due to the complexation between the fluorescers (i.e., HA, TC) and the quenchers (i.e., HMs and MPs) (Tang et al., 2019). The fluorescence quenching effect was quite remarkable in the ternary systems of TC-HMs-MPs and HA-HMs-MPs, with further reduction in the fluorescence intensity of either TC or HA (Fig. 6f; Figs. S9 and S10). This observation is likely due to the formation of new bridging complexes between TC or HA and HMs over the surface of MPs, in agreement with earlier reports (Nguyen et al., 2022; Li et al., 2018b; Wang et al., 2021b). Likewise, the 3D-EEM fluorescence spectrum of the real SW indicated the presence of both the fulvic-like and the humic-like compounds (Fig. S11a). The characteristic fluorescence spots of both compounds appeared to be effectively quenched by trace Cu^{2+} and Zn^{2+} (Figs. S11b–d), indicative of the complexation between HMs and the fulvic-like and humic-like compounds in real swine wastewaters, and probable bridging complexation between HMs and these compounds over the surface of MPs when coexisting in the real swine wastewaters.

Collectively, the mechanisms of Cu^{2+} or Zn^{2+} adsorption over the surface of aged MPs are proposed (Fig. 6g), with Coulomb attraction and surface complexation dominated in the absence of either TC or HA (left), and with bridging complexation occurring in the presence of either TC or HA. However, further works to identify the molecular configuration and the fractions of such bridging complexes using X-ray absorption spectroscopy are needed to verify the mechanisms proposed above.

4. Conclusions

In summary, MPs have a great affinity toward heavy metals (e.g., Cu^{2+} and Zn^{2+} ions), thereof appear to accumulate and spread such contaminants in simulated swine wastewater at environmentally relevant concentrations. Weathering can significantly accelerate the fragmentation of pristine MPs and endow the aged MPs with a variety of oxygen-containing functional groups, which appear to act as new active sites for binding both Cu^{2+} and Zn^{2+} ions. In addition, co-occurring humic acid and tetracycline species seem to facilitate the adsorption of heavy metals over the aged MPs via bridging complexation, which in consequence increases the risk of combined contamination and co-exposure, particularly in the case of co-occurring tetracycline. The co-occurring nutrients (e.g., phosphate and ammonia), however, demonstrated different impacts on Cu^{2+} and Zn^{2+} ions, with improved sequestration of Cu^{2+} ions by precipitation but lower immobilization for Zn^{2+} due to the formation of soluble zinc ammine complexes. These findings provided important insights into the interactions between aged MPs and heavy metal ions in specific environmentally relevant scenarios, and how the interactions are impacted by the intrinsic features of MPs and the environmental factors (e.g., pH, ionic strength, co-occurring species). However, further studies to examine the transport and fate of these heavy metal-loaded MPs are needed in particular when a strategy of nutrient recovery (e.g., struvite crystallization) was applied to such nutrient-rich swine wastewater to elucidate the mediating role of MPs for spreading heavy metals and/or tetracycline to the reclaimed value-added products (e.g., fertilizer).

CRediT authorship contribution statement

Mengyu Ma: Writing – original draft, Visualization, Methodology, Investigation. **Ruxin Han:** Visualization, Investigation. **Ruoqi Han:** Visualization, Investigation. **Defu Xu:** Investigation. **Feihu Li:** Writing – review & editing, Writing – original draft, Visualization, Supervision, Conceptualization.

Declaration of competing interest

The authors declare that they have no known competing financial interests or personal relationships that could have appeared to influence the work reported in this paper.

Data availability

Data will be made available on request.

Acknowledgments

The work was partially supported by the Innovation Training Programme for Undergraduate Students of NUIST (XJDC202310300164). We would like to acknowledge Nanjing Tianxiang Ecological Park for providing the actual swine wastewater.

Appendix A. Supplementary data

Supplementary data to this article can be found online at https://doi.org/10.1016/j.envpol.2024.124685.

References

Abdurahman, A., Cui, K.Y., Wu, J., Li, S.C., Gao, R., Dai, J., Liang, W.Q., Zeng, F., 2020. Adsorption of dissolved organic matter (DOM) on polystyrene microplastics in aquatic environments: kinetic, isotherm and site energy distribution analysis. Ecotoxicol. Environ. Saf. 198, 110658 https://doi.org/10.1016/j.ecoenv.2020.110658.

Al Harraq, A., Brahana, P.J., Arcemont, O., Zhang, D., Valsaraj, K.T., Bharti, B., 2022. Effects of weathering on microplastic dispersibility and pollutant uptake capacity. Acs Environ. Au 2, 549–555. https://doi.org/10.1021/acsenvironau.2c00036.

Alimi, O.S., Budarz, J.F., Hernandez, L.M., Tufenkji, N., 2018. Microplastics and nanoplastics in aquatic environments: aggregation, deposition, and enhanced contaminant transport. Environ. Sci. Technol. 52, 1704–1724. https://doi.org/10.1021/acs.est.7b05559.

Ateia, M., Apul, O.G., Shimizu, Y., Muflihah, A., Yoshimura, C., Karanfil, T., 2017. Elucidating adsorptive fractions of natural organic matter on carbon nanotubes. Environ. Sci. Technol. 51, 7101–7110. https://doi.org/10.1021/acs.est.7b01279.

Bah, A.T., Shen, Z.Y., Yan, J.N., Li, F.H., 2023. Phosphorous recovery from water via batch adsorption enrichment combined with struvite crystallization in a fluidized bed reactor. J. Environ. Chem. Eng. 11, 110180 https://doi.org/10.1016/j.jece.2023.110180.

Barhoumi, B., Metian, M., Oberhaensli, F., Mourgkogiannis, N., Karapanagioti, H.K., Bersuder, P., Tolosa, I., 2023. Extruded polystyrene microplastics as a source of brominated flame retardant additives in the marine environment: long-term field and laboratory experiments. Environ. Int. 172, 107797 https://doi.org/10.1016/j.envint.2023.107797.

Barnes, D.K.A., Galgani, F., Thompson, R.C., Barlaz, M., 2009. Accumulation and fragmentation of plastic debris in global environments. Philos. Trans. R. Soc. B Biol. Sci. 364, 1985–1998. https://doi.org/10.1098/rstb.2008.0205.

Binda, G., Spanu, D., Monticelli, D., Pozzi, A., Bellasi, A., Bettinetti, R., Carnati, S., Nizzetto, L., 2021. Unfolding the interaction between microplastics and (trace) elements in water: a critical review. Water Res. 204, 117637 https://doi.org/10.1016/j.watres.2021.117637.

Bradney, L., Wijesekara, H., Palansooriya, K.N., Obadamudalige, N., Bolan, N.S., Ok, Y.S., Rinklebe, J., Kim, K.H., Kirkham, M.B., 2019. Particulate plastics as a vector for toxic trace-element uptake by aquatic and terrestrial organisms and human health risk. Environ. Int. 131, 104937 https://doi.org/10.1016/j.envint.2019.104937.

Brennecke, D., Duarte, B., Paiva, F., Cacador, I., Canning-Clode, J., 2016. Microplastics as vector for heavy metal contamination from the marine environment. Estuar. Coast Shelf Sci. 178, 189–195. https://doi.org/10.1016/j.ecss.2015.12.003.

Chen, Y.J., Li, J.N., Wang, F.H., Yang, H., Liu, L., 2021. Adsorption of tetracyclines onto polyethylene microplastics: a combined study of experiment and molecular dynamics simulation. Chemosphere 265, 129133. https://doi.org/10.1016/j.chemosphere.2020.129133.

Chen, C., Wei, F., Ye, L., Wang, Y.T., Long, L.L., Xu, C.L., Xiao, Y.L., Wu, J., Xu, M., He, J. S., Yang, G., 2022. Adsorption of Cu^{2+} by UV aged polystyrene in aqueous solution. Ecotoxicol. Environ. Saf. 232, 113292 https://doi.org/10.1016/j.ecoenv.2022.113292.

Cole, M., Lindeque, P., Halsband, C., Galloway, T.S., 2011. Microplastics as contaminants in the marine environment: a review. Mar. Pollut. Bull. 62, 2588–2597. https://doi.org/10.1016/j.marpolbul.2011.09.025.

Cozar, A., Echevarria, F., Gonzalez-Gordillo, J.I., Irigoien, X., Ubeda, B., Hernandez-Leon, S., Palma, A.T., Navarro, S., Garcia-de-Lomas, J., Ruiz, A., Fernandez-de-Puelles, M.L., Duarte, C.M., 2014. Plastic debris in the open ocean. Proc. Natl. Acad. Sci. U.S.A. 111, 10239–10244. https://doi.org/10.1073/pnas.1314705111.

Dong, X.S., Liu, X.B., Hou, Q.L., Wang, Z.H., 2023. From natural environment to animal tissues: a review of microplastics (nanoplastics) translocation and hazards studies. Sci. Total Environ. 855, 158686 https://doi.org/10.1016/j.scitotenv.2022.158686.

Duan, J.J., Bolan, N., Li, Y., Ding, S.Y., Atugoda, T., Vithanage, M., Sarkar, B., Tsang, D. C.W., Kirkham, M.B., 2021. Weathering of microplastics and interaction with other coexisting constituents in terrestrial and aquatic environments. Water Res. 196, 117011 https://doi.org/10.1016/j.watres.2021.117011.

Frazier, A.W., Dillard, E.F., Lehr, J.R., 1975. System ammonia-zinc oxide-orthophosphoric acid-pyrophosphoric acid-water at 25. J. Agric. Food Chem. 23, 330–334. https://doi.org/10.1021/jf60198a038.

Fu, Q.M., Tan, X.F., Ye, S.J., Ma, L.L., Gu, Y.L., Zhang, P., Chen, Q., Yang, Y.Y., Tang, Y. Q., 2021. Mechanism analysis of heavy metal lead captured by natural-aged microplastics. Chemosphere 270, 128624. https://doi.org/10.1016/j.chemosphere.2020.128624.

Gao, L., Fu, D., Zhao, J., Wu, W., Wang, Z., Su, Y., Peng, L., 2021. Microplastics aged in various environmental media exhibited strong sorption to heavy metals in seawater. Mar. Pollut. Bull. 169, 112480 https://doi.org/10.1016/j.marpolbul.2021.112480.

Gardette, M., Perthue, A., Gardette, J.L., Janecska, T., Foldes, E., Pukanszky, B., Therias, S., 2013. Photo- and thermal-oxidation of polyethylene: comparison of mechanisms and influence of unsaturation content. Polym. Degrad. Stabil. 98, 2383–2390. https://doi.org/10.1016/j.polymdegradstab.2013.07.017.

Geyer, R., Jambeck, J.R., Law, K.L., 2017. Production, use, and fate of all plastics ever made. Sci. Adv. 3, e1700782 https://doi.org/10.1126/sciadv.1700782.

Goldberg, S., 2014. Application of surface complexation models to anion adsorption by natural materials. Environ. Toxicol. Chem. 33, 2172–2180. https://doi.org/10.1002/etc.2566.

Guan, J.N.A., Qi, K., Wang, J.Y., Wang, W.W., Wang, Z.R., Lu, N., Qu, J., 2020. Microplastics as an emerging anthropogenic vector of trace metals in freshwater: significance of biofilms and comparison with natural substrates. Water Res. 184, 116205 https://doi.org/10.1016/j.watres.2020.116205.

Ho, W.K., Law, J.C.F., Lo, J.C.W., Chng, I.K.X., Hor, C.H.H., Leung, K.S.Y., 2023. Sorption behavior, speciation, and toxicity of microplastic-bound chromium in multisolute systems. Environ. Sci. Technol. Lett. 10, 27–32. https://doi.org/10.1021/acs.estlett.2c00689.

Huang, X., Zemlyanov, D.Y., Diaz-Amaya, S., Salehi, M., Stanciu, L., Whelton, A.J., 2020. Competitive heavy metal adsorption onto new and aged polyethylene under various drinking water conditions. J. Hazard Mater. 385, 121585 https://doi.org/10.1016/j.jhazmat.2019.121585.

Huang, X.W., Ye, Z.L., Cai, J.S., Lin, L.F., 2021. Quantification of DOM effects on tetracyclines transport during struvite recovery from swine wastewater. Water Res. 206, 117756 https://doi.org/10.1016/j.watres.2021.117756.

Kadac-Czapska, K., Knez, E., Grembecka, M., 2024. Food and human safety: the impact of microplastics. Crit. Rev. Food Sci. Nutr. 64, 3502–3521. https://doi.org/10.1080/10408398.2022.2132212.

Khan, A.R., Ulhassan, Z., Li, G.L., Lou, J.B., Iqbal, B., Salam, A., Azhar, W., Batool, S., Zhao, T.T., Li, K.X., Zhang, Q.Y., Zhao, X., Du, D.L., 2024. Micro/nanoplastics: critical review of their impacts on plants, interactions with other contaminants (antibiotics, heavy metals, and polycyclic aromatic hydrocarbons), and management strategies. Sci. Total Environ. 912, 169420 https://doi.org/10.1016/j.scitotenv.2023.169420.

Koelmans, A.A., Bakir, A., Burton, G.A., Janssen, C.R., 2016. Microplastic as a vector for chemicals in the aquatic environment: critical review and model-supported reinterpretation of empirical studies. Environ. Sci. Technol. 50, 3315–3326. https://doi.org/10.1021/acs.est.5b06069.

Lee, Y.K., Hong, S., Hur, J., 2021. A fluorescence indicator for source discrimination between microplastic-derived dissolved organic matter and aquatic natural organic matter. Water Res. 207, 117833 https://doi.org/10.1016/j.watres.2021.117833.

Li, J.Y., Liu, H.H., Chen, J.P., 2018a. Microplastics in freshwater systems: a review on occurrence, environmental effects, and methods for microplastics detection. Water Res. 137, 362–374. https://doi.org/10.1016/j.watres.2017.12.056.

Li, S.C., Liu, H., Gao, R., Abdurahman, A., Dai, J., Zeng, F., 2018b. Aggregation kinetics of microplastics in aquatic environment: complex roles of electrolytes, pH, and natural organic matter. Environ. Pollut. 237, 126–132. https://doi.org/10.1016/j.envpol.2018.02.042.

Li, X.W., Mei, Q.Q., Chen, L.B., Zhang, H.Y., Dong, B., Dai, X.H., He, C.Q., Zhou, J., 2019. Enhancement in adsorption potential of microplastics in sewage sludge for metal pollutants after the wastewater treatment process. Water Res. 157, 228–237. https://doi.org/10.1016/j.watres.2019.03.069.

Li, Y., Wang, X.J., Wang, Y., Sun, Y., Xia, S.Q., Zhao, J.F., 2022. Effect of biofilm colonization on Pb(II) adsorption onto poly(butylene succinate) microplastic during its biodegradation. Sci. Total Environ. 833, 155251 https://doi.org/10.1016/j.scitotenv.2022.155251.

Lin, L.J., Tang, S., Wang, X.S., Sun, X., Liu, Y., 2021. Sorption of tetracycline onto hexabromocyclododecane/polystyrene composite and polystyrene microplastics: statistical physics models, influencing factors, and interaction mechanisms. Environ. Pollut. 284, 117164 https://doi.org/10.1016/j.envpol.2021.117164.

Liu, Y.H., Kwag, J.H., Kim, J.H., Ra, C.S., 2011. Recovery of nitrogen and phosphorus by struvite crystallization from swine wastewater. Desalination 277, 364–369. https://doi.org/10.1016/j.desal.2011.04.056.

Liu, P., Qian, L., Wang, H.Y., Zhan, X., Lu, K., Gu, C., Gao, S.X., 2019. New insights into the aging behavior of microplastics accelerated by advanced oxidation processes. Environ. Sci. Technol. 53, 3579–3588. https://doi.org/10.1021/acs.est.9b00493.

Liu, P., Zhan, X., Wu, X.W., Li, J.L., Wang, H.Y., Gao, S.X., 2020a. Effect of weathering on environmental behavior of microplastics: properties, sorption and potential risks. Chemosphere 242, 125193. https://doi.org/10.1016/j.chemosphere.2019.125193.

Liu, Y.J., Huang, Z.Q., Zhou, J.N., Tang, J., Yang, C., Chen, C.Y., Huang, W.L., Dang, Z., 2020b. Influence of environmental and biological macromolecules on aggregation kinetics of nanoplastics in aquatic systems. Water Res. 186, 116316 https://doi.org/10.1016/j.watres.2020.116316.

Lu, X.T., Zeng, F., Wei, S.Y., Gao, R., Abdurahman, A., Wang, H., Liang, W.Q., 2022. Effects of humic acid on Pb^{2+} adsorption onto polystyrene microplastics from spectroscopic analysis and site energy distribution analysis. Sci. Rep. 12, 8932. https://doi.org/10.1038/s41598-022-12776-3.

Ma, J., Qiu, Y., Zhao, J.Y., Ouyang, X.X., Zhao, Y.J., Weng, L.P., Yasir, A.M., Chen, Y.L., Li, Y.T., 2022. Effect of agricultural organic inputs on nanoplastics transport in saturated goethite-coated porous media: particle size selectivity and role of dissolved organic matter. Environ. Sci. Technol. 56, 3524–3534. https://doi.org/10.1021/acs.est.1c07574.

Ma, M., Li, F., 2023. Insights into the adsorption of copper/zinc ions over aged polyethylene and polyethylene terephthalate microplastics. ChemRixv. https://doi.org/10.26434/chemrxiv-2023-q52xg.

Ma, X.Y., Ma, X.L., Chen, P., 2023. The effect of microplastics-plants on the bioavailability of copper and zinc in the soil of a sewage irrigation area. Bull. Environ. Contam. Toxicol. 110, 58. https://doi.org/10.1007/s00128-022-03674-5.

Mao, R.F., Lang, M.F., Yu, X.Q., Wu, R.R., Yang, X.M., Guo, X.T., 2020. Aging mechanism of microplastics with UV irradiation and its effects on the adsorption of heavy metals. J. Hazard Mater. 393, 122515 https://doi.org/10.1016/j.jhazmat.2020.122515.

Meng, F., Ma, W., Wang, Y., Zhu, Z., Chen, Z., Lu, G., 2020. A tribo-positive Fe@MoS2 piezocatalyst for the durable degradation of tetracycline: degradation mechanism and toxicity assessment. Environ. Sci.: Nano 7, 1704–1718. https://doi.org/10.1039/d0en00284d.

Nguyen, T.B., Ho, T.B.C., Huang, C., Chen, C.W., Chen, W.H., Hsieh, S.C., Hsieh, S.L., Dong, C.D., 2022. Adsorption of lead(II) onto PE microplastics as a function of particle size: influencing factors and adsorption mechanism. Chemosphere 304, 135276. https://doi.org/10.1016/j.chemosphere.2022.135276.

Paul, M.B., Stock, V., Cara-Carmona, J., Lisicki, E., Shopova, S., Fessard, V., Braeuning, A., Sieg, H., Bohmert, L., 2020. Micro- and nanoplastics - current state of knowledge with the focus on oral uptake and toxicity. Nanoscale Adv. 2, 4350–4367. https://doi.org/10.1039/d0na00539h.

Pérez, O., Odio, O.F., Reguera, E., 2022. XPS as a probe for the bonding nature in metal acetates. New J. Chem. 46, 11255–11265. https://doi.org/10.1039/d2nj01905a.

Qiao, R.X., Lu, K., Deng, Y.F., Ren, H.Q., Zhang, Y., 2019. Combined effects of polystyrene microplastics and natural organic matter on the accumulation and toxicity of copper in zebrafish. Sci. Total Environ. 682, 128–137. https://doi.org/10.1016/j.scitotenv.2019.05.163.

Reineccius, J., Schönke, M., Waniek, J.J., 2023. Abiotic long-term simulation of microplastic weathering pathways under different aqueous conditions. Environ. Sci. Technol. 57, 963–975. https://doi.org/10.1021/acs.est.2c05746.

Shabbir, S., Faheem, M., Dar, A.A., Ali, N., Kerr, P.G., Yu, Z.G., Li, Y., Frei, S., Albasher, G., Gilfedder, B.S., 2022. Enhanced periphyton biodegradation of endocrine disrupting hormones and microplastic: intrinsic reaction mechanism, influential humic acid and microbial community structure elucidation. Chemosphere 293, 133515. https://doi.org/10.1016/j.chemosphere.2022.133515.

Shen, Z.Y., Jin, J., Fu, J.J., Yang, M., Li, F.H., 2021. Anchoring Al- and/or Mg-oxides to magnetic biochars for Co-uptake of arsenate and fluoride from water. J. Environ. Manag. 293, 112898 https://doi.org/10.1016/j.jenvman.2021.112898.

Sparks, D.L., Singh, B., Siebecker, M.G., 2023. Chapter 5 - sorption phenomena on soils. In: Sparks, D.L., Singh, B., Siebecker, M.G. (Eds.), Environmental Soil Chemistry, third ed. Academic Press, Boston, pp. 203–281.

Tang, J., Zhuang, L., Yu, Z., Liu, X.M., Wang, Y.Q., Wen, P., Zhou, S.G., 2019. Insight into complexation of Cu(II) to hyperthermophilic compost-derived humic acids by EEM-PARAFAC combined with heterospectral two dimensional correlation analyses. Sci. Total Environ. 656, 29–38. https://doi.org/10.1016/j.scitotenv.2018.11.357.

Tian, W.J., Song, P.A., Zhang, H.Y., Duan, X.G., Wei, Y., Wang, H., Wang, S.B., 2023. Microplastic materials in the environment: problem and strategical solutions. Prog. Mater. Sci. 132, 101035 https://doi.org/10.1016/j.pmatsci.2022.101035.

Tong, F., Liu, D., Zhang, Z.H., Chen, W., Fan, G.P., Gao, Y., Gu, X.Y., Gu, C., 2023. Heavy metal-mediated adsorption of antibiotic tetracycline and ciprofloxacin on two microplastics: insights into the role of complexation. Environ. Res. 216, 114716 https://doi.org/10.1016/j.envres.2022.114716.

Torres, F.G., Dioses-Salinas, D.C., Pizarro-Ortega, C.I., De-la-Torre, G.E., 2021. Sorption of chemical contaminants on degradable and non-degradable microplastics: recent progress and research trends. Sci. Total Environ. 757, 143875 https://doi.org/10.1016/j.scitotenv.2020.143875.

Town, R.M., van Leeuwen, H.P., Duval, J.F.L., 2023. Effect of polymer aging on uptake/release kinetics of metal ions and organic molecules by micro- and nanoplastics: implications for the bioavailability of the associated compounds. Environ. Sci. Technol. 57, 16552–16563. https://doi.org/10.1021/acs.est.3c05148.

Upadhyay, R., Singh, S., Kaur, G., 2022. Sorption of pharmaceuticals over microplastics' surfaces: interaction mechanisms and governing factors. Environ. Monit. Assess. 194, 803. https://doi.org/10.1007/s10661-022-10475-0.

Wang, F.Y., Yang, W.W., Cheng, P., Zhang, S.Q., Zhang, S.W., Jiao, W.T., Sun, Y.H., 2019. Adsorption characteristics of cadmium onto microplastics from aqueous solutions. Chemosphere 235, 1073–1080. https://doi.org/10.1016/j.chemosphere.2019.06.196.

Wang, F., Wang, B., Duan, L., Zhang, Y.Z., Zhou, Y.T., Sui, Q., Xu, D.J., Qu, H., Yu, G., 2020a. Occurrence and distribution of microplastics in domestic, industrial, agricultural and aquacultural wastewater sources: a case study in Changzhou. Water Res. China 182, 115956. https://doi.org/10.1016/j.watres.2020.115956.

Wang, Q.J., Zhang, Y., Wangjin, X.X., Wang, Y.L., Meng, G.H., Chen, Y.H., 2020b. The adsorption behavior of metals in aqueous solution by microplastics effected by UV radiation. J. Environ.Sci. China 87, 272–280. https://doi.org/10.1016/j.jes.2019.07.006.

Wang, Y.H., Yang, Y.N., Liu, X., Zhao, J., Liu, R.H., Xing, B.S., 2021a. Interaction of microplastics with antibiotics in aquatic environment: distribution, adsorption, and toxicity. Environ. Sci. Technol. 55, 15579–15595. https://doi.org/10.1021/acs.est.1c04509.

Wang, Y., Wang, X.J., Li, Y., Li, J., Liu, Y.Y., Xia, S.Q., Zhao, J.F., 2021b. Effects of exposure of polyethylene microplastics to air, water and soil on their adsorption behaviors for copper and tetracycline. Chem. Eng. J. 404, 126412 https://doi.org/10.1016/j.cej.2020.126412.

Wang, X.X., Zhang, R.X., Li, Z.Y., Yan, B., 2022. Adsorption properties and influencing factors of Cu(II) on polystyrene and polyethylene terephthalate microplastics in seawater. Sci. Total Environ. 812, 152573 https://doi.org/10.1016/j.scitotenv.2021.152573.

Wu, R.T., Cai, Y.F., Chen, Y.X., Yang, Y.W., Xing, S.C., Liao, X.D., 2021. Occurrence of microplastic in livestock and poultry manure in South China. Environ. Pollut. 277, 116790 https://doi.org/10.1016/j.envpol.2021.116790.

Wu, C., Tanaka, K., Tani, Y., Bi, X.Y., Liu, J.L., Yu, Q.Q., 2022. Effect of particle size on the colonization of biofilms and the potential of biofilm-covered microplastics as metal carriers. Sci. Total Environ. 821, 153265 https://doi.org/10.1016/j.scitotenv.2022.153265.

Yan, J.N., Ma, M.Y., Zhao, B., Li, F.H., 2023. Phosphate recovery from wastewater by rapid adsorption-desorption enrichment over UiO-66@melamine sponge composites. J. Water Process Eng. 55, 104253 https://doi.org/10.1016/j.jwpe.2023.104253.

Yang, K., Miao, G.F., Wu, W.H., Lin, D.H., Pan, B., Wu, F.C., Xing, B.S., 2015. Sorption of Cu^{2+} on humic acids sequentially extracted from a sediment. Chemosphere 138, 657–663. https://doi.org/10.1016/j.chemosphere.2015.07.061.

Yang, J., Cang, L., Sun, Q., Dong, G., Ata-Ul-Karim, S.T., Zhou, D.M., 2019. Effects of soil environmental factors and UV aging on Cu^{2+} adsorption on microplastics. Environ. Sci. Pollut. Res. 26, 23027–23036. https://doi.org/10.1007/s11356-019-05643-8.

Yu, F., Li, Y., Huang, G.Q., Yang, C.F., Chen, C., Zhou, T., Zhao, Y.C., Ma, J., 2020. Adsorption behavior of the antibiotic levofloxacin on microplastics in the presence of different heavy metals in an aqueous solution. Chemosphere 260, 127650. https://doi.org/10.1016/j.chemosphere.2020.127650.

Zhang, Z.Y., Liu, H.J., Wu, L.Y., Lan, H.C., Qu, J.H., 2015. Preparation of amino-Fe(III) functionalized mesoporous silica for synergistic adsorption of tetracycline and copper. Chemosphere 138, 625–632. https://doi.org/10.1016/j.chemosphere.2015.07.014.

Zhang, S.W., Li, Y.X., Chen, X.C., Jiang, X.M., Li, J., Yang, L., Yin, X.Q., Zhang, X.L., 2022. Occurrence and distribution of microplastics in organic fertilizers in China. Sci. Total Environ. 844, 157061 https://doi.org/10.1016/j.scitotenv.2022.157061.

Zhao, G.X., Li, J.X., Ren, X.M., Chen, C.L., Wang, X.K., 2011. Few-layered graphene oxide nanosheets as superior sorbents for heavy metal ion pollution management. Environ. Sci. Technol. 45, 10454–10462. https://doi.org/10.1021/es203439v.

Zhao, Y.F., Gao, J.F., Wang, Z.Q., Dai, H.H., Wang, Y.W., 2021. Responses of bacterial communities and resistance genes on microplastics to antibiotics and heavy metals in sewage environment. J. Hazard Mater. 402, 123550 https://doi.org/10.1016/j.jhazmat.2020.123550.

Zhou, W.S., Han, Y., Tang, Y., Shi, W., Du, X.Y., Sun, S.G., Liu, G.X., 2020. Microplastics aggravate the bioaccumulation of two waterborne veterinary antibiotics in an edible bivalve species: potential mechanisms and implications for human health. Environ. Sci. Technol. 54, 8115–8122. https://doi.org/10.1021/acs.est.0c01575.

Zhu, D., Xinag, Q., Yang, X.R., Ke, X., O'Connor, P., Zhu, Y.G., 2019. Trophic transfer of antibiotic resistance genes in a soil detritus food chain. Environ. Sci. Technol. 53, 7770–7781. https://doi.org/10.1021/acs.est.9b00214.

Zou, J.Y., Liu, X.P., Zhang, D.M., Yuan, X., 2020. Adsorption of three bivalent metals by four chemical distinct microplastics. Chemosphere 248, 126064. https://doi.org/10.1016/j.chemosphere.2020.126064.